Supplement: Electron - optical phonon coupling in suspended graphene bilayer

Antti Laitinen[1], Manohar Kumar[1], Mika Oksanen[1], Bernard Plaçais[2,1], Pauli Virtanen[1], and Pertti Hakonen[1]
[1]*Low Temperature Laboratory, O.V. Lounasmaa Laboratory, Aalto University, 00076 AALTO, Finland and*
[2]*Laboratoire Pierre Aigrain, Ecole Normale Supérieure, CNRS (UMR8551), Université Pierre et Marie Curie, Université Paris Diderot, 75231 Paris Cedex 05, France*
(Dated: March 20, 2015)

I. SAMPLE FABRICATION AND CHARACTERIZATION

Initially, we employed HF-etching in order to make graphene suspended[1], but later we switched to the technique introduced in Ref. 2, the LOR-technique. This technique was selected over the conventional HF-technique, because of the lower parasitic pad capacitance that can be achieved, which is important for our microwave measurements. The lower parasitic capacitance is due to longer distance between the graphene circuit and the strongly doped Si^{++} back gate.

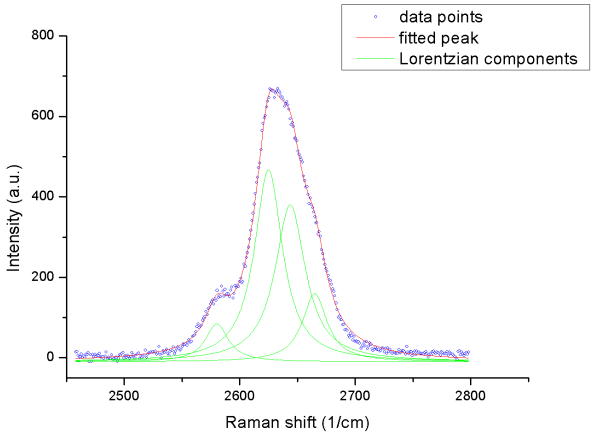

Figure S1. 2D peak in a Raman spectrum of a suspended sample fabricated with the LOR-method. The red trace displays a sum of four fitted Lorentzian indicated in green.

Compared to a Raman spectrum of a sample directly on SiO_2 with the standard D, G and 2D peaks, there are some additional features in a spectrum of a sample on LOR. Near 1600 1/cm, where one expects to see G-peak characteristic for carbon and 1350 1/cm D-peak associated with defects, there are a few other peaks. Origin of these peaks is unclear, but since the sample performance with these LOR-samples has been good compared to HF-etched samples, it can be assumed that the peaks originate from the LOR-layer. Additionally, the D-peak is virtually nonexistent which implies very few defects in the graphene, as verified by the high mobility of the samples. Around 2600 1/cm, where one observes the 2D peak used to determine the number of layers, there are no excess peaks visible. However, the measured widths of the 2D-peaks for samples on LOR tend to be slightly larger than expected (*i.e.* in comparison with the samples on SiO_2). Fig. S1 displays the 2D peak of a bilayer sample suspended using the LOR technique.

II. NOISE

Shot noise S_I measured up to high bias is illustrated in terms of the Fano factor in Fig. S2. The Fano factor is determined for excess noise: $F = (S_I(I) - S_I(0))/2eI$, where $S_I(I)$ and $S_I(0)$ denote the current noise power spectrum at current I and at $I = 0$, respectively. Near the Dirac point, there is a slight initial increase of F in sample S1, which reflects tendency towards the hot electron regime as the effective strength of the electron-electron interaction becomes enhanced with growing bias[3–5]. On the other hand, the Fano factor of sample S2 indicates an immediate decrease with bias, which is a sign of inelastic processes entering already at low energies, for example due to sliding modes in bilayer graphene[6]; this inelastic scattering is observed even in the differential conductance of sample S2 in Fig. 3 of the main paper where the linear increase with bias voltage is cut off earlier than in sample S1. Pretty smooth, symmetric decrease in F is observed with the bias voltage over the full range of bias conditions; moreover, no difference in F at equal hole and electron density was found so that there is no difference in e-ph coupling for the electron and hole transport regimes.

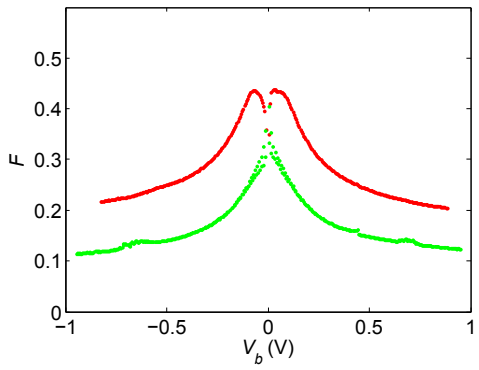

Figure S2. Excess Fano factor F vs. bias voltage V near the charge neutrality point at charge density $n \simeq 1.0 \cdot 10^{10}$ cm^{-2}. The red curve represents sample S1 and the green one corresponds to sample S2.

III. DETAILS OF THE ELECTRICAL CHARACTERISTICS

In our experiments, we measured the electrical characteristics of the samples both at DC and at low-frequency AC (dynamic resistance $R_d = dV/dI$). IV-curves of S1 measured at the charge density $n = 1.0 \cdot 10^{10}$ cm^{-2} and $n = 2.8 \cdot 10^{11}$ cm^{-2} are illustrated in Fig. S3. The IV-curve displays a clear decrease in $R_\square = (V/I)W/L$ with growing bias voltage V around the Dirac point. The differential resistance $R_d = dV/dI$, measured by lock-in methods, corresponds to the inverse slope of the IV-curve. The $R_d(V)$ measurements were employed to determine the coupling strength of the current noise from the sample to the preamplifier at microwave frequencies. The behavior of $R_\square$ as a function of shot noise temperature T_e is illustrated in Fig. S4 at the same charge densities as the IV curves in Fig. S3. The temperature dependence of $R_\square$ is well fit at $T_e \lesssim 100$ K using $C\log(T_e)$ where the prefactor $C \simeq 390 - 890$ Ω. When the fitted $C\log(T_e)$ part is subtracted off from $R_\square$, we obtain for the difference $\Delta R_\square$ an almost linear dependence on T_e. This behavior suggests that the scattering rate by optical phonons grows nearly linearly above $300 - 400$ K, which is in agreement with recent single layer calculations of Ref. 7 without electron-electron interaction effects and with the non-suspended bilayer analysis of Ref. 8.

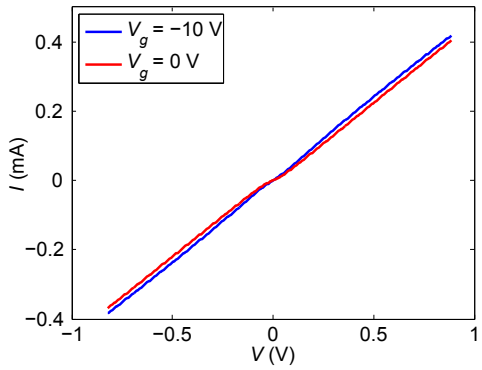

Figure S3. Current I vs. bias voltage V around the Dirac point at charge density $n = 1.0 \cdot 10^{10}$ cm^{-2} (red) and $n = 2.8 \cdot 10^{11}$ cm^{-2} (blue) for sample S1.

Note that linear $R(T)$ is predicted for in-plane acoustic phonons (see e.g. Ref. 9) but these cannot be the dominant processes because of the results on the electron phonon coupling. The $\log(T_e)$ dependence may be due to very robust weak localization effects[10] or it may be a signature of increased effective disorder[11]; the disorder may cause logarithmic increase in conductance as a function of (disorder length scale)$^{-1}$.

IV. ANALYSIS OF THE POWER LAWS

In order to support the conclusion of electron - optical phonon scattering, let us plot the data of Fig. 4 in the main paper in a slightly different form. For acoustic phonons or supercollision processes, the heat flow from electrons to the phonons would be approximately characterized by the power law $P \propto T_e^\delta$ (here we have dropped the small phonon temperature term T_{ph}^δ) where δ would be 2 or 3, respectively. The law with $\delta = 2$ can be ruled out immediately without any doubt. For the supercollision case with $\delta = 3$, we compare our results with the theory by replotting our data in the same way as in the experimental works on supercollisions in graphene[12–14]: Fig. S5 displays the original data of Fig. 4 in the main paper by normalizing the power flow P_e with T_e^3. No clear saturation is observed to signify $\delta = 3$ behavior. As a reference we have plotted the behavior for electron - optical phonon scattering, which reproduces the asymptotic features of the data. Clearly, the shape of the curve follows the thermally activated optical phonon tendency which is characteristic to the formation of modes with well defined energy.

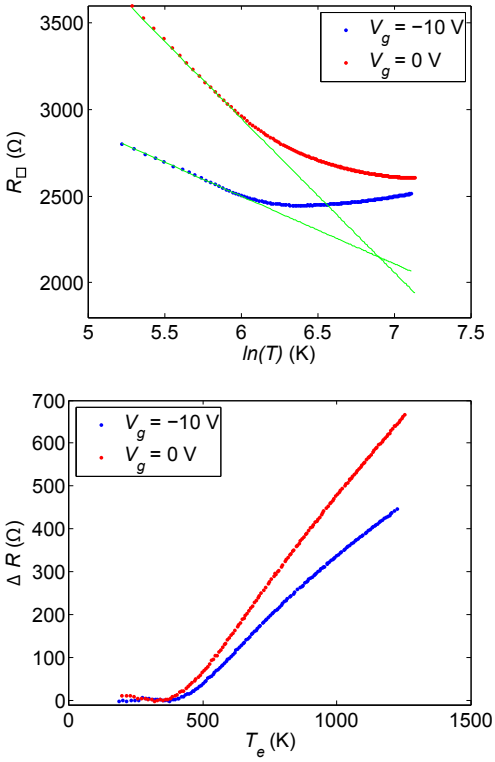

Figure S4. a) Total sheet resistance $R_\square = (V/I)W/L$ as a function of the logarithm of the electronic temperature deduced from the Fano factor using $T_e = Fe|V|/2k_B$ (at $1.0{\cdot}10^{10}$ cm^{-2} and at $|n| = 2.8 \cdot 10^{11}$ cm^{-2}) for sample S1. The green lines indicate logarithmic temperature dependence at low temperature. b) Deviation from the logarithmic behavior $R_\square - C\log(T_e)$ for the two data sets in the upper frame.

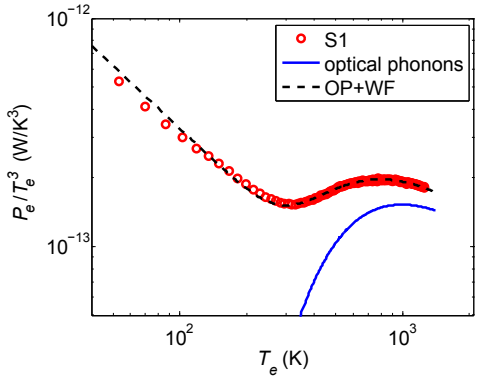

Figure S5. Measured heat flow from electrons to phonons (data S1 from Fig. 4 in the main text) normalized by T_e^3 and displayed as a function of T_e. The dashed curve illustrates the theoretical curve from Fig. 4 (left frame) of the main paper. The blue curve denotes the heat flow due to the optical phonon scattering alone, while the dashed curve contains additionally the electronic heat conduction.

The dependence of the electron phonon coupling on the chemical potential is illustrated in Fig. S6 for sample S1. We find a weak variation with chemical potential which we assign to the variation in electrical resistance of the sample. The dashed curve in Fig. S6 displays the sum of the theoretical electron phonon coupling and the electronic part for heat conduction which was obtained from the measured electrical resistance $R(V_g)$, symmetrized at high bias, and the Wiedemann-Franz law. The slightly stronger measured variation compared with the theoretical curve might be an indication of mass renormalization due to interactions[15] although these effects are expected to be small.

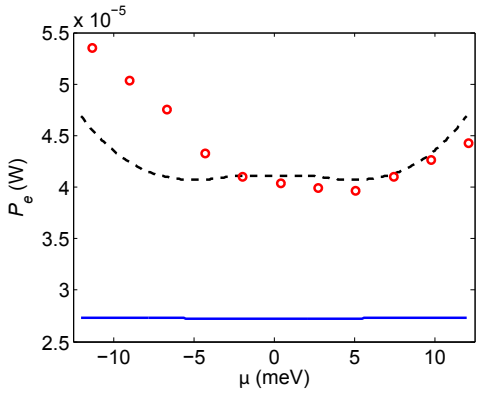

Figure S6. Chemical potential dependence of the measured heat flow from electrons to phonons at $T_e = 600$ K for sample S1. The dashed line indicates the theoretical variation obtained using the change in the electronic heat conduction on top of the optical-phonon-facilitated heat flow which is denoted by the blue curve[16,17].

[1] K. I. Bolotin, K. J. Sikes, J. Hone, H. L. Stormer, and P. Kim, Phys. Rev. Lett. **101**, 096802 (2008).

[2] N. Tombros, A. Veligura, J. Junesch, J. Jasper van den Berg, P. J. Zomer, M. Wojtaszek, I. J. Vera Marun, H. T. Jonkman, and B. J. van Wees, J. Appl. Phys. **109**, 093702 (2011).

[3] A. H. Steinbach, J. M. Martinis, and M. H. Devoret, Phys. Rev. Lett. **76**, 3806 (1996).

[4] K. E. Nagaev, Phys. Rev. B **52**, 4740 (1995).

[5] J. Sarkar, *Microwave experiments and noise in mesoscopic devices*, Ph.D. thesis, Aalto University (2015), (unpublished).

[6] C.-H. Park, F. Giustino, M. L. Cohen, and S. G. Louie, Nano Lett. **8**, 4229 (2008).

[7] C.-H. Park, N. Bonini, T. Sohier, G. Samsonidze, B. Kozinsky, M. Calandra, F. Mauri, and N. Marzari, Nano Lett. **14**, 1113 (2014).

[8] A. Fay, R. Danneau, J. K. Viljas, F. Wu, M. Y. Tomi, J. Wengler, M. Wiesner, and P. J. Hakonen, Phys. Rev. B **84**, 245427 (2011).

[9] E. Hwang and S. Das Sarma, Phys. Rev. B **77**, 115449 (2008).

[10] F. V. Tikhonenko, D. W. Horsell, R. V. Gorbachev, and A. K. Savchenko, Phys. Rev. Lett. **100**, 056802 (2008).

[11] J. Tworzydło, C. W. Groth, and C. W. J. Beenakker, Phys. Rev. B **78**, 235438 (2008).

[12] A. C. Betz, S. H. Jhang, E. Pallecchi, R. Ferreira, G. Fève, J.-M. Berroir, and B. Plaçais, Nat. Phys. **9**, 109 (2012).

[13] A. C. Betz, F. Vialla, D. Brunel, C. Voisin, M. Picher, A. Cavanna, A. Madouri, G. Fève, J.-M. Berroir, B. Plaçais, and E. Pallecchi, Phys. Rev. Lett. **109**, 056805 (2012).

[14] A. Laitinen, M. Oksanen, A. Fay, D. Cox, M. Tomi, P. Virtanen, and P. Hakonen, Nano Lett. **14**, 3009 (2014).

[15] G. Borghi, M. Polini, R. Asgari, and A. H. MacDonald, Solid State Commun. **149**, 1117 (2009).

[16] R. Bistritzer and A. H. MacDonald, Phys. Rev. Lett. **102**, 206410 (2009).

[17] J. K. Viljas and T. T. Heikkilä, Phys. Rev. B **81**, 245404 (2010).